JOC The Journal of Organic Chemistry

Article

pubs.acs.org/joc

Photoinduced Isomerization of 23-Oxosapogenins: Conformational Analysis and Spectroscopic Characterization of 22-Isosapogenins

Izabella Jastrzębska,[†] Marcin Górecki,[‡] Jadwiga Frelek,[‡] Rosa Santillan,[§] Leszek Siergiejczyk,[†] and Jacek W. Morzycki*,[†]

[†]Institute of Chemistry, University of Białystok, Piłsudskiego 11/4, 15-443 Białystok, Poland

[‡]Institute of Organic Chemistry, Polish Academy of Sciences, Kasprzaka 44/52, 01-224 Warsaw, Poland

[§]Departamento de Química, CINVESTAV-IPN, Apdo. Postal 14-740, 07000 México, D.F., Mexico

Supporting Information

ABSTRACT: The first synthesis of 22-isospirostane derivatives is described. They were obtained by photochemical isomerization of 23-oxosapogenins. The structure of 23-oxo-22-isotigogenin acetate (**12**) was proved by a single crystal X-ray diffraction, while structures of 23-oxo-22-isodiosgenin acetate (**13**) and 23-oxo-22-isosarsasapogenin acetate (**14**) were elucidated by spectroscopic methods. 22-Isodiosgenin acetate (**17**) was obtained by $NaBH_4$ reduction of the 23-oxo derivative **13** followed by the two-step Barton−McCombie deoxygenation procedure. Conformational analysis of 22-iso compounds was carried out with CD and NMR, as well as DFT calculations.

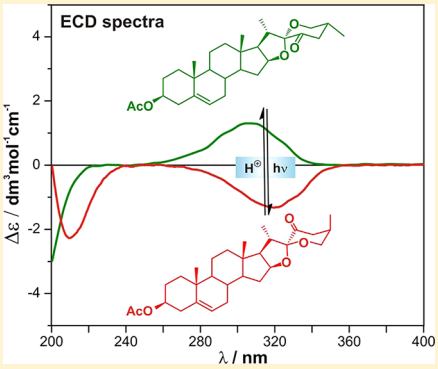

INTRODUCTION

Saponins are a class of compounds found in natural sources, particularly abundant in various plant species with different, sometimes beneficial, biological activities.[1] More specifically, they are amphiphilic glycosides composed of one or more hydrophilic glycoside moieties combined with a lipophilic triterpene or steroid derivative. The glycoside-free portions (aglycones) of the saponins are termed sapogenins. The steroid sapogenins are cholestane, furostane, or spirostane derivatives. The latter compounds with the two additional spiro connected rings (E and F) are the most frequently found in plants. The normal-type configuration at the spiro carbon atom (such as in diosgenin) was found in the majority of naturally occurring compounds. The 21-methyl group is usually α-oriented (20*S*). However, the spirostanes differ in configuration at C25. In compounds with an equatorial 27α-methyl group (e.g., diosgenin (**1**), tigogenin (**3**), smilagenin (**5**), hecogenin (**7**)) it is *R*, while compounds with an axial 27β-methyl group (e.g., yamogenin (**2**), neotigogenin (**4**), sarsasapogenin (**6**), silalagenin (**8**)), have the 25*S* configuration (Figure 1).

Of course, there are also further structural differences between the saponins in the type of functionalization and configuration at the A/B ring junction (5α- and 5β-steroids). Apart from the most common sapogenins with a [4.5] spiroketal system, in nature exist the isomeric [4.4] spiroketal compounds with both configurations (*R* or *S*) at the spiro carbon atom (Figure 2). The chemistry of spirostanes was intensively studied during the past century.[2] Plant sapogenins are relatively cheap raw materials for syntheses, usually employing the Marker degradation,[3] of a number of medicinally important steroids.[4] Recently, spirostanes have been enjoying a renaissance due to the intensive studies on cephalostatins and ritterazines.[5]

RESULTS AND DISCUSSION

With regard to a question of [4.5] spiroketal configuration, it should be noticed that there are three stereogenic centers (C20, C22, and C25) in the side chain, and as a consequence, eight stereoisomers can be formed. The molecular mechanics calculations show that normal (natural) sapogenins (22*R*) have lower steric energy than their epimers at the spiro carbon atom. The reason for that is the repulsion between binding electrons of angular 18-methyl group and lone pair electrons on the F-ring oxygen in the isomeric spiroketal systems. In addition to that, there is only one anomeric effect in the isomeric compounds compared to two such effects in normal [4.5] spiroketals. Also, the natural configuration at C20 (20*S*) is preferred over the isomeric one, since the 20*R* isomers show higher steric energy. Finally, compounds with an equatorial methyl group at C25 (25*R*) are more stable than their axial 25*S* isomers. Therefore, of the eight possible stereoisomers, the 20*S*,22*R*,25*R*-spirostanes are the thermodynamically most stable ones.[6] If the reaction conditions enable interconversion between the isomers, these compounds are preferentially formed (e.g., compounds **1**, **3**, **5**, **7** of Figure 1).

Received: October 28, 2012
Published: November 28, 2012

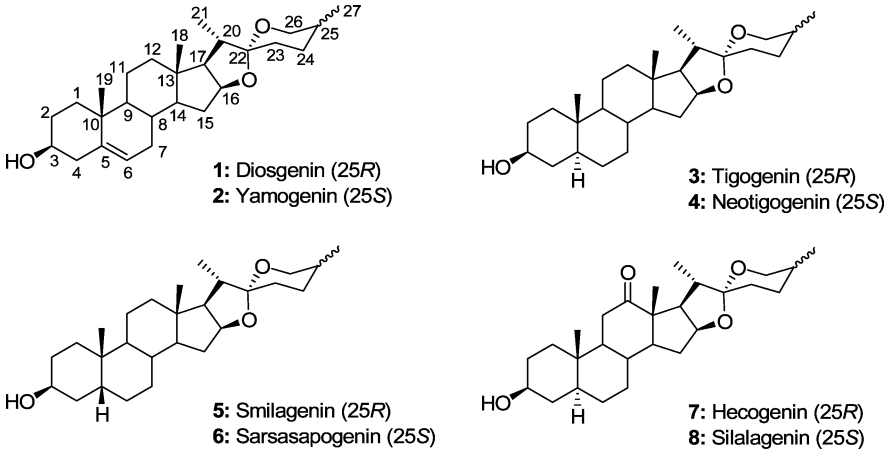

Figure 1. Structures of common spirostane sapogenins.

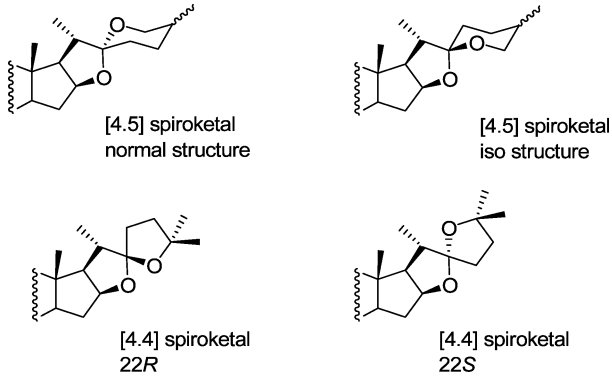

Figure 2. Spiroketal and pseudosapogenin structures.

The isomerization reactions between the [4.5] spiroketal sapogenins are well-known. In acid medium, protonation (acylation, Lewis acid complexation) of sapogenins at the oxygen atom of ring F occurs followed by cleavage of the ring affording enol ethers commonly called pseudosapogenins (Figure 3).[7] The reaction is reversible, and starting sapogenins are formed from pseudosapogenins on treatment with strong proton acids. Under these conditions (thermodynamic control) the original configuration at C20 and C22 is restored, since the 20*S*,22*R* spiroketal system is the most stable. However, if a weak acid (e.g., acetic acid) is used, the kinetically favored products are formed. Then the product distribution depends on configuration at C25. In the case of 25*R* pseudosapogenins, the major product is the compound with inverted configuration at C20. A similar transformation of tigogenin (**3**) to its 20*R* epimer can be also achieved electrochemically.[8]

The 25*S* pseudosapogenins preferentially afford the 20*R*,22*S* product (inversion of configurations at both chiral centers) in addition to the parent sapogenin and its epimer at C20.

Treatment of the 25*S* sapogenins with strong proton or Lewis acids leads to formation of 25*R* sapogenins (e.g., isomerization of sarsasapogenin (**6**) to smilagenin (**5**)).[6,9] This unique transformation has previously been explained in terms of an oxidation−reduction mechanism (Figure 4).[10] The key step of the process is a reversible 1,5-hydride transfer from C26 to C22.

The isomerization involves a series of equilibria between the oxonium ions produced by acid. The driving force of the reaction is a formation of a more stable product with an equatorial (25*R*) methyl group.

None of the known isomerization methods allow a change in configuration at the spiro carbon atom without alteration of configuration at other side chain chiral centers. It seems that sapogenins with the 22-isomeric [4.5] spiroketal structure do not occur in nature, though there are a few reports in the literature about isolation of such compounds. The last example

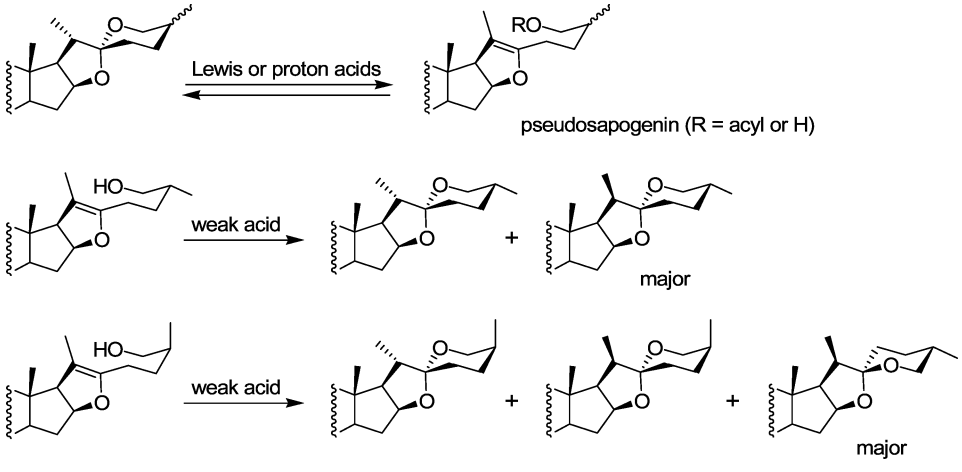

Figure 3. Ring-closure reactions of pseudosapogenins.

dx.doi.org/10.1021/jo3022549 | J. Org. Chem. 2012, 77, 11257−11269

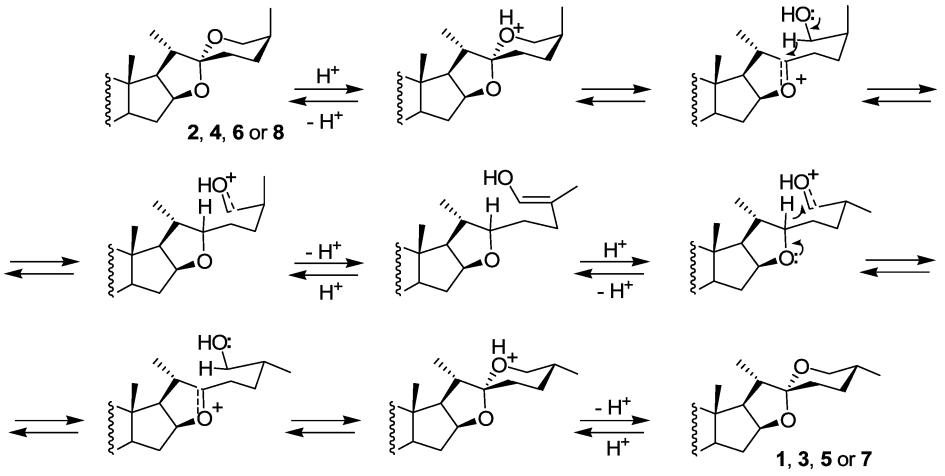

Figure 4. Acid-catalyzed isomerization of sapogenins at C-25.

Scheme 1

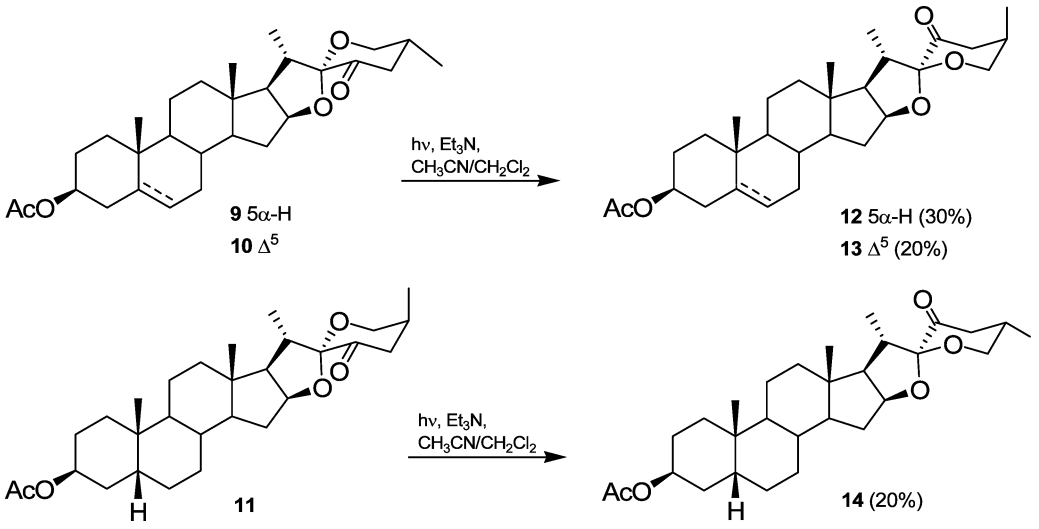

is the structure of cephalostatin 16,[11] but the proposed structure has been questioned later.[12]

The problem with the synthesis of the 22-isomeric [4.5] spiroketal system is its thermodynamic instability. It is, however, a challenge for synthetic chemists, especially as high-energy stereoisomers frequently show high biological activities.[5a,13]

Here we present the photochemical isomerization of spirostanes with a carbonyl group at C23 position.

The ketones **9**, **10** and **11** (Scheme 1) were prepared from naturally occurring sapogenins: diosgenin (**1**), tigogenin (**3**) and sarsasapogenin (**6**), respectively. The starting sapogenins **1**, **3**, and **6** have the *R* configuration at the spiro carbon atom, but oxygenation at C23 formally inverts configuration at C22 because of the change in priority between substituents (C20 and C23). The sapogenins were oxidized to the corresponding 23-oxoderivatives by Barton's procedure,[14] improved by Iglesias-Arteaga.[15] UV irradiations of 23-ketones **9**−**11** were carried out in acetonitrile/dichloromethane solutions in the presence of triethylamine at room temperature for 1−2 h. Under the described conditions, slow isomerization occurred at the spiro (C22) carbon atom to the slightly more polar isomers **12**, **13** and **14**. However, the photochemical equilibrium could not be reached since highly polar overirradiation products were formed (the reactions were monitored by TLC and stopped when a spot at the bottom of the TLC plate suggested intolerably high concentrations of such products). From the reaction mixtures, substantial amounts of starting compounds **9**, **10**, and **11** were recovered (40, 60, and 44%, respectively).

The products **12**−**14** proved isomeric with the starting compounds as it was shown by MS-ESI. In the ^{13}C NMR spectra a signal at 203.8 ppm (compounds **12** and **13**) or 202.5 ppm (compound **14**) confirmed the presence of a carbonyl group in the obtained products. The 26-H signal pattern in the ^{1}H NMR spectra of compounds **10**, **11**, **13**, and **14** is different for each compound and can be used for distinguishing between the isomers (Figure 5). Of course, the presence of the C5−C6 double bond or lack of such bond has little influence on 26-H signals, and therefore, the spectra in the diagnostic range were virtually identical for compounds **9** and **10** (δ 3.5−3.9 ppm) and for compounds **12** and **13** (δ 3.5−4.3 ppm). The starting sapogenins with the 25*R* configuration (i.e., with the equatorial methyl group at C25), 23-oxotigogenin acetate (**9**) and 23-oxodiosgenin acetate (**10**) show 26-H signals less separated from each other than in the case of the 25*S* compound with the axial methyl group, 23-oxosarsasapogenin acetate (**11**). In the case of 23-oxodiosgenin acetate (**10**), the signals arose as a triplet at 3.79 ppm (axial H pro-*R*, J = 11.2 Hz) and a doublet

dx.doi.org/10.1021/jo3022549 | J. Org. Chem. 2012, 77, 11257−11269

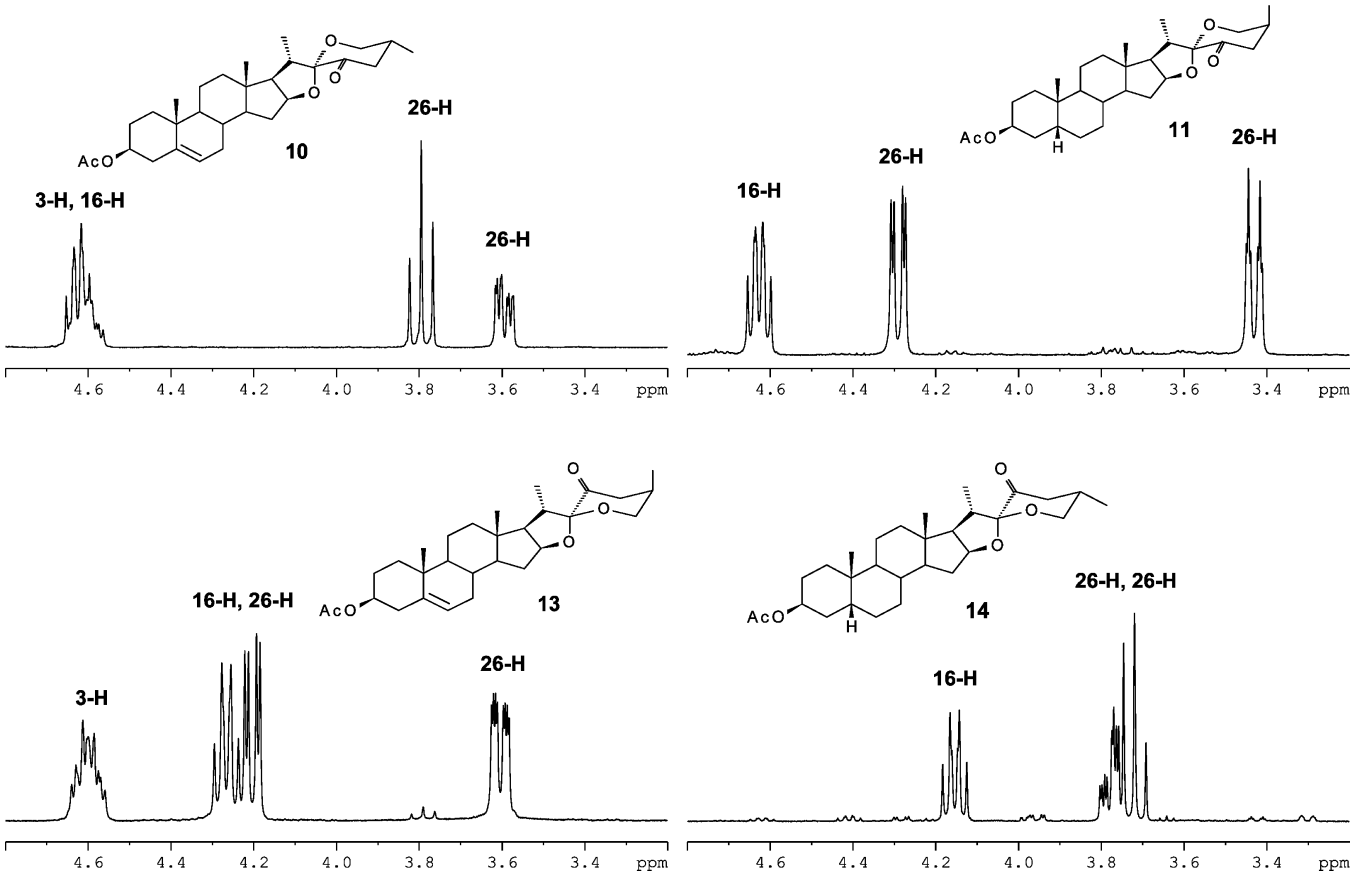

Figure 5. Selected ^{1}H NMR signals of starting materials (**10**, **11**) and products (**13**, **14**).

of doublets of doublets at 3.59 ppm (equatorial H pro-*S*, *J* = 11.2, 5.0, 1.7 Hz), while in the case of 23-oxosarsasapogenin acetate (**11**), these two signals showed up at 4.28 ppm (axial H pro-*R*, doublet of doublets, *J* = 11.2, 2.9 Hz) and 3.42 ppm (equatorial H pro-*S*, doublet of triplets, *J* = 11.1, 2.1 Hz). The 26-H signal patterns proved symptomatic for the 22-isomeric systems. In 23-oxo-22-isodiosgenin acetate (**13**), a doublet of doublets of doublets was observed at 3.60 ppm (axial H pro-*S*, *J* = 11.2, 3.8, and 1.8 Hz) and a doublet of doublets at 4.20 ppm (equatorial H pro-*R*, *J* = 11.2 and 3.4 Hz). For 23-oxo-22-isosarsasapogenin acetate (**14**), in turn, the 26-H signals appeared as a doublet of doublets of doublets at 3.78 ppm (equatorial H pro-*R*, *J* = 11.3, 4.6, 1.9 Hz) and a triplet at 3.72 ppm (axial H pro-*S*, *J* = 11.3 Hz).

The described above coupling constants of 26-H unequivocally prove the position (axial or equatorial) of the methyl group at C25. It is obvious that during photochemical reactions, configuration at this chiral center remains intact. Assuming that isomerizations occur at the spiro carbon atom and the ring F chair conformation dominates, the methyl group at C25 must be axial in the product **13**, unlike the starting 23-oxodiosgenin acetate (**10**). Similarly, it was expected to be equatorial in the case of the product **14**, while in the starting 23-oxosarsasapogenin acetate (**11**) the 25-methyl group occupied the axial position. These predictions were confirmed by analysis of signals at 26-H.[16]

The structure of product **12** (Figure 6), obtained by irradiation of 23-oxotigogenin acetate (**9**), was unequivocally proved by an X-ray analysis. An inversion of configuration at

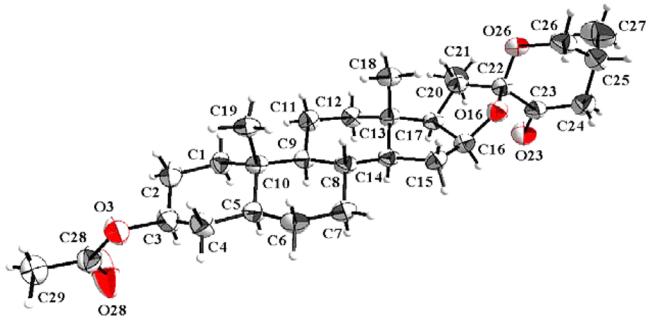

Figure 6. Molecular structure of **12** with displacement ellipsoids drawn at the 35% probability level.

C22 (the spiro carbon atom) during the photo reaction was confirmed.

The X-ray crystal structure analysis established that the six-membered A, B and C rings adopt the expected chair conformation, while the five-membered D ring shows a half-chair conformation and the E ring displays an envelope conformation. The pyran ring F shows a chair conformation, and it was also possible to establish the configuration at C22 and C25 being both *R*, with the methyl at C25 in axial orientation. The methyl group in **12** occupies the axial position both in solid state and in solution as proved by the ^{1}H NMR spectrum of **12**, which showed a similar pattern of 26-H signals to that presented for the compound **13**.

A strong confirmation of the structural features of spirosapogenins discussed above is provided by experimental and theoretical circular dichroism spectra (CD). Since CD

dx.doi.org/10.1021/jo3022549 | *J. Org. Chem.* 2012, 77, 11257−11269

Table 1. UV and ECD Data of Compounds 9−14 Recorded in CH_3CN

comp	UV ε (λ_{max})		ECD $\Delta\varepsilon$ (λ_{max})		
9		31 (299.0)	−4.2 (196.5)		+1.3 (306.0)
10	11400 (191.4)	33 (299.0)	−10.2 (186.0)		+1.3 (306.0)
11	2650 (199.0)	47 (302.5)	−3.4 (196.0)		+1.6 (310.0)
12		95 (316.0)	+3.8 (190.0)	−2.3 (210.0)	−1.3 (321.0)
13	12100 (192.6)	93 (316.0)	+3.4 (196.0)[a]	−1.5 (214.0)	−1.3 (320.0)
14	2590 (200.5)	77 (316.0)	+2.6 (190.0)	−1.8 (211.0)	−0.6 (320.0)

[a]An additional band with $\Delta\varepsilon$ equal to −3.7 is present at 185 nm.

spectroscopy is very sensitive to the small changes in the geometry and electronic structure of the investigated molecules, the combination of experimental and theoretical CD results should allow the drawing of more definite conclusions within the scope of present research. Such combination has already proven efficient and reliable for the assignment of the absolute configuration of various chiral organic molecules.[17]

The experimental electronic circular dichroism (ECD) spectra of spirosapogenins **9**−**14** were measured at room temperature in acetonitrile and thus represent a thermal average over the ECD spectra of different conformers. In terms of ECD results, **9**−**14** can be divided into two groups. The first group, consisting of compounds **9**−**11**, exhibits two ECD bands, whereas the second group, containing compounds **12**−**14**, possesses three ECD bands in the same spectral region (Table 1, Figure 7). The sign and position of the carbonyl nπ* band clearly depends on the configuration of the spiro carbon atom (C22). And so, in compounds **9**−**11** with 22*S* absolute configuration, this ECD band occurs at around 310 nm and is positive, while in the case of compounds **12**−**14** with the 22*R* absolute configuration it has a negative sign and is shifted toward the red to about 320 nm. For the first group the ECD band attributed to the $\pi\pi$* carbonyl transition and arising at around 190 nm has the opposite sign to the nπ* band; i.e., it is negative. For the second group, however, the band in this spectral range is bisignate with two maxima of opposite signs: a negative one at ca. 210 nm and a positive one at around 190 nm. These bands are a mixture of excitations out of the carbonyl transitions and transitions out of acetate carbonyl and oxygen lone pairs into the same acceptor orbitals (see the Supporting Information).

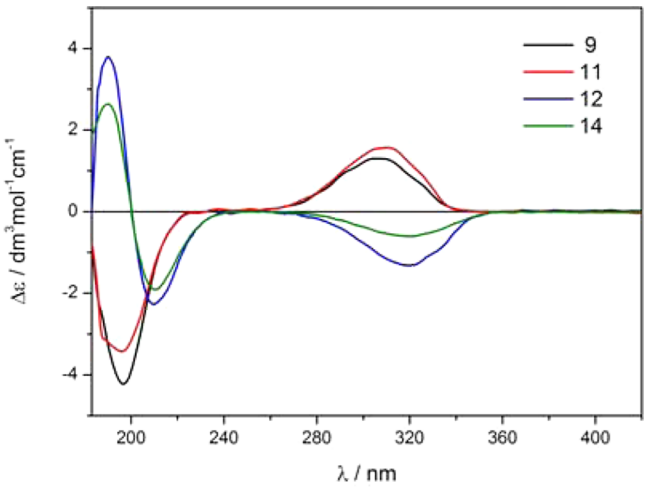

Figure 7. ECD spectra of compounds **9** (black), **11** (red), **12** (blue) and **14** (green) measured in CH_3CN.

In principle, ECD spectra are identical for compounds **9**, **10** and **12**, **13** differing only in the presence or absence of the double bond at C5−C6. However, the transitions out of the double bond orbitals mix strongly with the carbonyl transitions, and for **10**, this mixing results in strong absorption at 186 nm. In the case of **13**, in turn, the absorption at 196 nm can be attributed to transitions occurring within the double bond mostly (see the Supporting Information).

To rationalize the experimental observations, the TDDFT calculations using B3LYP/TZVP/PCM method were performed for **10**−**14**. First, the applied calculation methodology was validated by direct comparison of the geometry-related data obtained from the X-ray studies and from the molecular modeling of spirosapogenin **12**.

For spirosapogenin **12**, two conformers within a 3 kcal/mol energy window were found (Figure 8). In the first one, populated in the conformational equilibrium over 78%, the six-membered ring F is in a chair conformation and the methyl group at C25 occupies an axial position. In the second conformer, higher in energy by 0.77 kcal/mol, this ring adopts a boat conformation with the methyl group at C25 in an equatorial position (Figure 8). The lowest energy chair conformer is in a very good agreement with solid state structure, as it is apparent from the data of Table 2 and comparison of structures in Figure 6 and 8 (left).

A very good agreement between the solid-state and computed structures (Table 2), as well as the close similarity of the ECD spectra of **12** recorded in both solid-state and

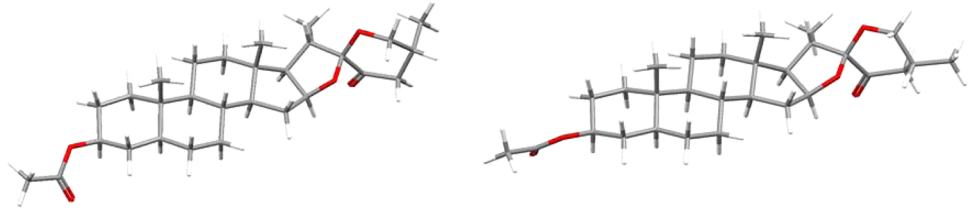

Figure 8. Structures of the ring F lowest energy chair conformer (left) and ring F boat conformer (right) of **12** calculated at the B3LYP/6-31G(d) level of theory.

dx.doi.org/10.1021/jo3022549 | J. Org. Chem. 2012, 77, 11257−11269

Table 2. Selected Torsional Angles in Deg (°) Determined by the X-ray Diffraction and Calculated for Lowest Energy Conformers of 10–14 by B3LYP/6-31G(d) Method[a]

comp		27–25–24–23	27–25–26–O26	O26–26–25–24	26–25–24–23	25–24–23–22	24–23–22–O26
10	calc.	173.49	−179.68	56.18	−49.43	48.51	−50.50
11	calc.	73.52	−66.48	57.23	−50.28	48.82	−50.21
12	X-ray	−77.59	67.15	−58.71	48.20	−38.91	39.30
	calc.	−78.03	65.78	−58.71	47.80	−39.40	38.69
13	calc.	−76.01	65.24	−58.61	47.78	−39.56	38.90
14	calc.	167.14	170.10	−67.15	44.29	−21.14	16.54

[a]Atom numbering as in Figure 6.

solution (Figure 9) indicates the presence of the same molecular species in both states. This means that the solute–solvent interactions, which may considerably affect the CD spectra because of both conformational and vicinal effects, are negligible in this case and point out that the observed ECD is largely a molecular property. Therefore, the analysis of the ECD data can be performed on the basis of chiroptical data obtained for solutions.

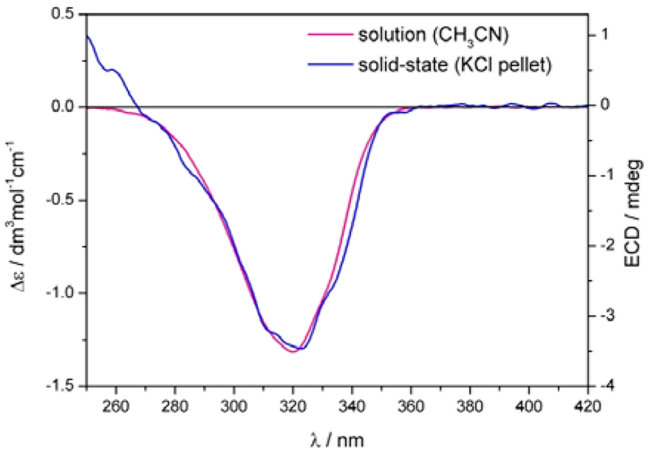

Figure 9. ECD spectra of spirosapogenin **12** recorded in acetonitrile (purple line) shown in $\Delta\varepsilon$ and in KCl pellet (blue line) given in mdeg, both presented over the range 380–250 nm.

To provide further evidence and to find experimental verification for the computational results, the variable low-temperature ECD spectra of spirosapogenin **12** were recorded. As can be seen in the resulting spectra, the intensity of the diagnostic nπ* band is greatly dependent on temperature of the solution (Figure 10). The spectra showed a decrease of the 320 nm band intensity with lowering the temperature. The experimental result is in line with the calculations, because the population of the lowest energy conformer with computed Cotton effects in the corresponding spectral regions should increase with decreasing temperature. Since the rotatory strength of chair conformer is substantially lower than that for boat conformer, the lowest energy chair conformer dominates at lower temperatures while contribution from boat conformer increases at higher temperatures (Table 3).

Table 3. Calculated (DFT) Population of Chair (Column A) and Boat (Column B) Conformers of 12 at Different Temperatures (In Percent)

temp (K)	A	B
298	78.7	21.3
273	80.6	19.4
233	84.2	15.8
193	88.3	11.7
153	92.7	7.3
113	96.9	3.1
93	98.5	1.5

The presented results clearly demonstrate that the conformational changes considerably affect ECD spectra, although the origin of calculated rotatory strengths remains the same.

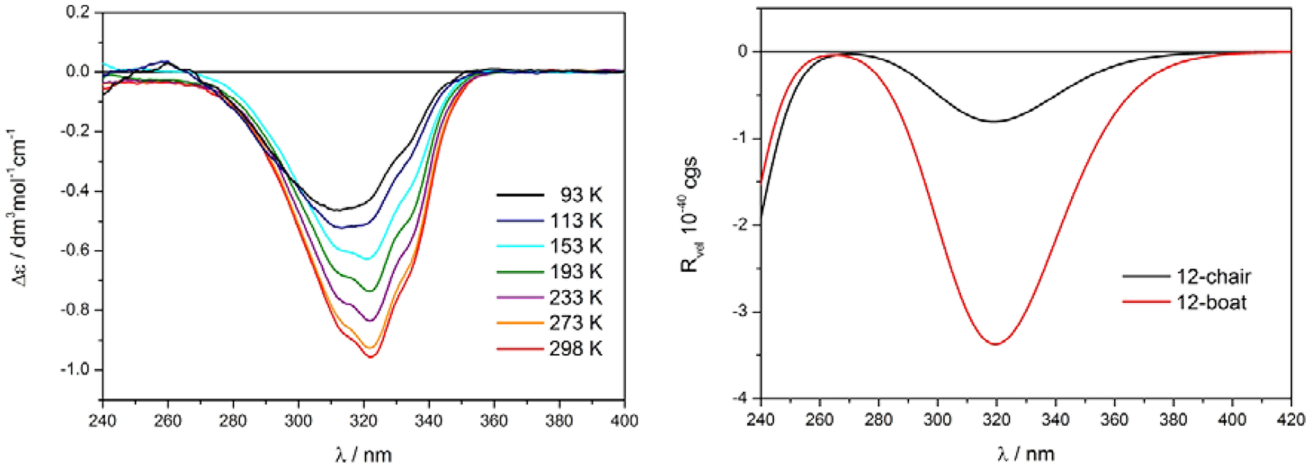

Figure 10. Left: Variable low-temperature ECD measurements of **12** recorded in MI_{13} (methylcyclohexane–isopentane, 1:3, by vol.). Right: Simulated ECD spectra of chair and boat conformers of **12** at the B3LYP/TZVP/PCM (2,2,4-trimethylpentane, ε = 1.936) level of theory.

dx.doi.org/10.1021/jo3022549 | J. Org. Chem. 2012, 77, 11257–11269

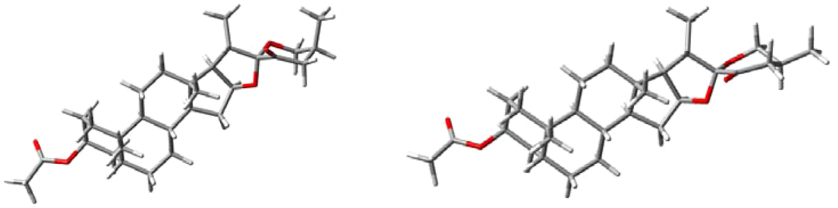

Figure 11. Structures of the two lowest energy conformers of **11** calculated at the B3LYP/6-31G(d) level of theory. Left, chair conformer; right, boat conformer.

The results for **12** demonstrate a very good conformity between the calculated and the solid-state values and prove the correctness of the calculation methodology used. Thus, for the remaining spirosapogenins, which do not form crystals suitable for the X-ray analysis, the same TDDFT calculation methodology was applied. The selected structural data for lowest energy conformers of compounds **10**–**14** are collected in Table 2.

For compound **11** representing the first group of spirosapogenins with the 22*S* absolute configuration, two conformers have been found in the energy range of 3 kcal·mol^{-1} (Figure 11). The lowest energy conformer belongs to the structural class characterized by a chair conformation of the six-membered ring F and an axial orientation of the methyl group at C25. Its population in the conformational equilibrium definitely prevails and amounts to 93.5%. The second stable conformer of higher energy by 1.58 kcal·mol^{-1}, populated in the conformational equilibrium in 6.5%, shows the six-member ring F in a boat conformation with the 25-methyl group in the equatorial position. In the Boltzmann-averaged ECD spectrum comprising, by definition, the sum of contributions from all populated conformers, two ECD bands of the negative sign at 203 nm and the positive one at 295 nm are visible (Figure 12).

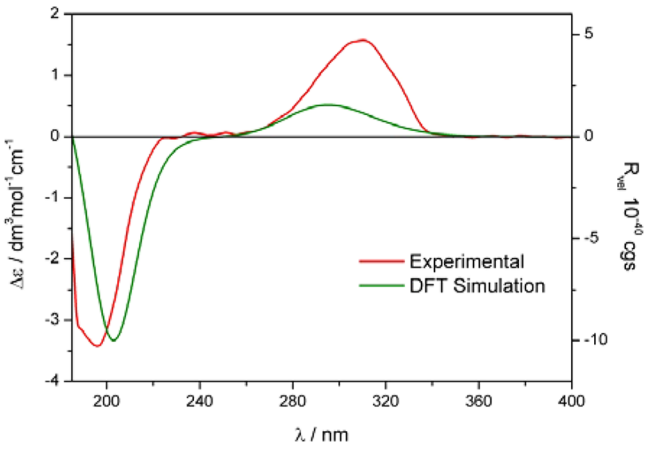

Figure 12. Computed ECD spectrum at the B3LYP/TZVP/PCM (CH_3CN) level of theory obtained as a population-weighted sum at 298 K of individual conformers of **11** compared to experiment in CH_3CN.

The Boltzmann-averaged spectrum shows very satisfactory agreement between experiment and theory, thus providing strong evidence that these conformers are present in solution under these conditions. Besides, this result identifies the chiral carbon atom C22 of **11** as being of *S* configuration.

Only one contributing conformer was found for compound **14** within a 3 kcal/mol energy window. In this conformer, the six-membered ring F is in a slightly skewed chair conformation and the methyl group at C25 occupies an equatorial position (Figure 13, left). The simulated ECD spectrum is in an excellent agreement with the experimental data. Thus, on the basis of the results of combined experimental and theoretical ECD analysis, the 22*R* absolute configuration can be assigned for **14** with a high degree of confidence. The results of calculations for spirosapogenins **10** and **13** are summarized in the Supporting Information.

The formation of irradiation products of 23-oxosapogenins may be readily explained, since the α-cleavage (Norrish type I)[18] of the C22–C23 bond is likely to occur in this system. A tentative mechanism for the photochemical isomerization of the 23-oxospirostanols is outlined in Scheme 2.

On irradiation of 23-oxosapogenins, an intermediate **A** is initially formed by α-cleavage. The C22 radical centers were also formed during our preceding study on photochemical reactions of 23-hydroxy sapogenins.[19] Such centers are stabilized by neighboring oxygen atoms and thus favorable. Since the radical at C22 is flat, the reconstruction of the C22–C23 bond by radical recombination may occur from either side affording the starting ketones (**9**–**11**) or products of their isomers at the spiro carbon atom (**12**–**14**).

Crystals of 23-oxo-22-isosapogenins are resistant to sun light exposition, but in solution (e.g., in dichloromethane) slow isomerization to the normal type sapogenin derivatives is observed. In the presence of a catalytic amount of *p*-TsOH the isomerization of 23-oxo-22-isosapogenin **13** into 23-oxo-diosgenin acetate (**10**) is much faster; a complete isomerization in dichloromethane occurs within 90 min at room temperature.

In the next step, attempts to remove the carbonyl group in 23-oxo-22-isodiosgenin **13** without affecting the configuration at the spiro carbon atom were undertaken. Since the Wolff–Kishner approach did not work because of the steric hindrance around the 23-carbonyl group (the 23-hydrazone was not formed), compound **13** was reduced with $NaBH_4$ to give a mixture of epimeric 23-alcohols **15** in comparable amounts. A relatively high content of the axial alcohol in the mixture is due to the easier approach of the hydride to the 23-carbonyl group from the side opposite to the axial methyl group at C25. On the other hand, the equatorial approach of hydride is hindered by the α-methyl group at C20.[20] The mixture of alcohols was then converted into mesylates followed by lithium aluminum hydride reduction. However, a difficult to separate mixture of several deoxygenated products was obtained. The most likely rearrangements of the spiroketal moiety during the hydride reduction occurred, as it was previously observed in the case of 23-mesylates in the normal spiro system.[21]

Finally, the mixture of 23-alcohols was subjected to the Barton–McCombie deoxygenation procedure.[22,23] In the first step xanthate **16** was prepared, albeit in a low yield. Interestingly, only the equatorial epimer of **16** was obtained. The large coupling constants of 23-H (J = 10.6 and 5.4 Hz)

dx.doi.org/10.1021/jo3022549 | J. Org. Chem. 2012, 77, 11257–11269

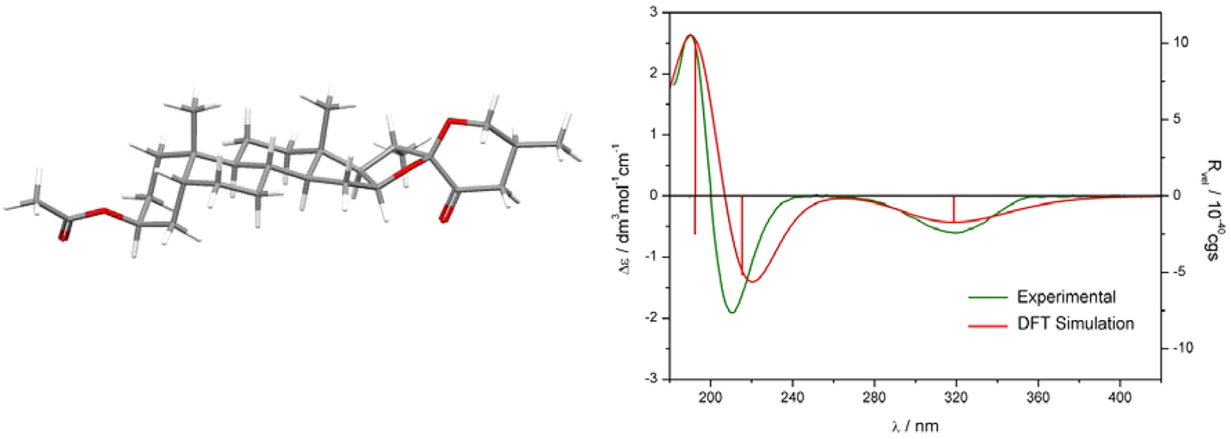

Figure 13. Structure of the lowest energy conformer of spirosapogenin **14** calculated at the B3LYP/6-31G(d) level of theory and its computed ECD spectrum at the B3LYP/TZVP/PCM (CH_3CN, ε = 35.688) level of theory compared to experiment in CH_3CN.

Scheme 2

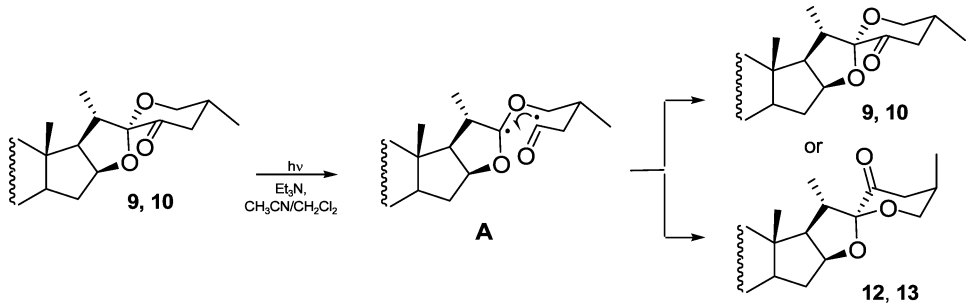

Scheme 3

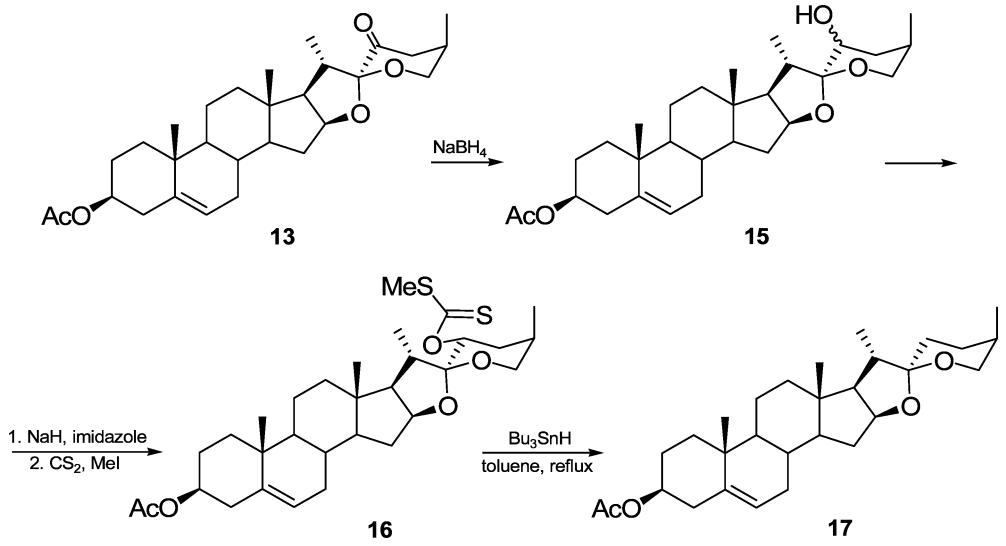

proved its axial orientation. Most likely the axial alcohol did not form the corresponding xanthate because of steric hindrance. The reductive displacement of the dithiocarbonate group of **16** with Bu_3SnH proceeded smoothly in toluene to afford the desired 22-isodiosgenin acetate (**17**). The reactions described are outlined in Scheme 3.

From the 26-H signal pattern of **17** it was easy to deduce the axial orientation of the methyl group at C25 (Figure 14). The signals were well separated (δ 4.06 and 3.38), similar to other compounds (**11**, **12**, **13**) with an axial methyl group at C25. The large geminal coupling constant (J = 11.2 Hz) was accompanied by much smaller ones between axial (J = 3.2 Hz) and equatorial (<1 Hz) protons at C26 and the equatorial proton at C25.

An isomerization reaction of 22-isodiosgenin acetate (**17**) into diosgenin acetate was carried out in the presence of *p*-TsOH in dichloromethane. The reaction was fast: about 75% of the starting material disappeared in 15 min. The reaction was completed within less than 1 h. It seems that isomerization of 22-isodiosgenin acetate (**17**) to the normal spiroketal system proceeds faster than in the case of its 23-oxo derivative **13**.

dx.doi.org/10.1021/jo3022549 | J. Org. Chem. 2012, 77, 11257−11269

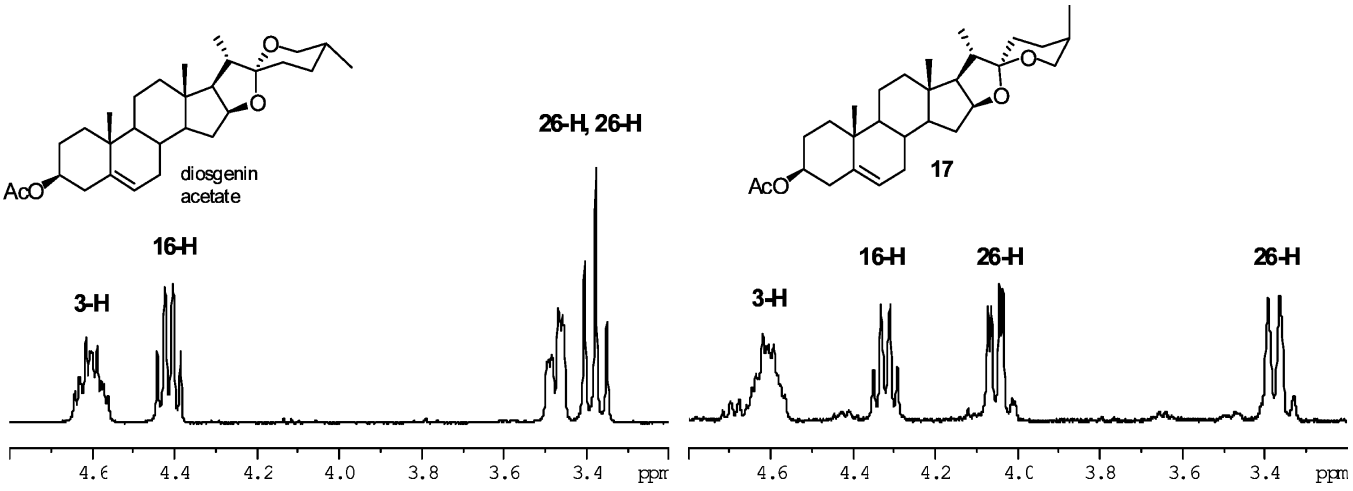

Figure 14. Selected ^{1}H NMR signals of diosgenin acetate and 22-isodiosgenin acetate (**17**).

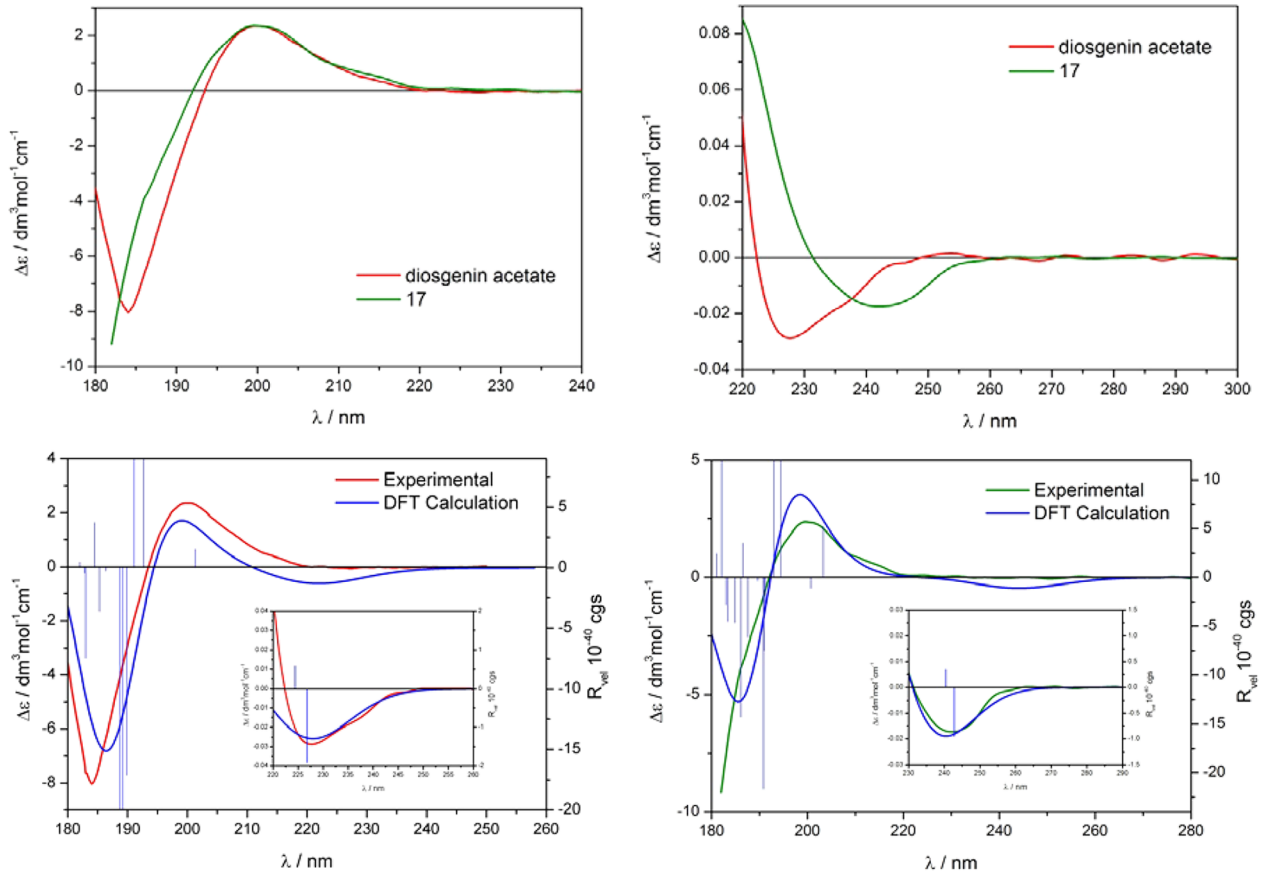

Figure 15. Top: ECD spectra of diosgenin acetate and 22-isodiosgenin acetate (**17**) measured in CH_3CN. Bottom: Comparison of experimental and simulated ECD spectra of diosgenin acetate (left) and 22-isodiosgenin acetate (**17**) (right).

To independently confirm the structure of 22-isodiosgenin acetate (**17**), CD spectroscopy was applied again. In fact, 22-isodiosgenin acetate (**17**) differs from diosgenin acetate only in the configuration at the spiro carbon atom (C22) and, as a consequence, in orientation of the 25-methyl group, which occupies in the former compound the axial position. Since both these compounds do not have a suitable chromophoric system, it could be expected that ECD spectra would not allow distinguishing between the isomers (Figure 15). Indeed, the ECD spectra of both compounds are very similar over the spectral range 180−220 nm. However, the observed shift of the long-wavelength band by 15 nm toward the red in **17** in comparison with diosgenin acetate correlates well with a similar red shift in spirosapogenins **12**−**14** compared to spirosapogenins **9**−**11**. This indicates the same absolute configuration at C22 for **17** and **12**−**14** and thus points to the absolute configuration of C22 as *S* in 22-isodiosgenin acetate (**17**). A very good agreement between the simulated and experimental ECD spectra lends strong support to this assignment (Figure 15).

dx.doi.org/10.1021/jo3022549 | J. Org. Chem. 2012, 77, 11257−11269

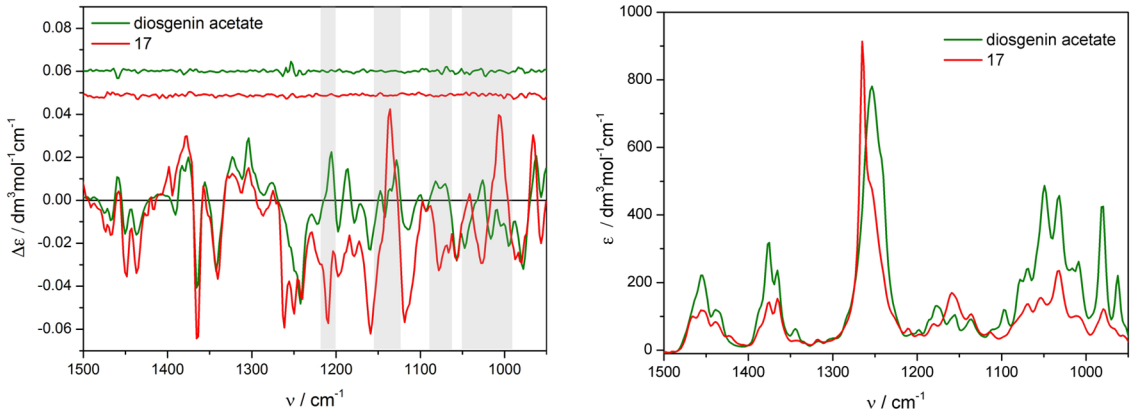

Figure 16. VCD (left) with noise level and IR spectra (right) of diosgenin acetate and 22-isodiosgenin acetate (**17**) measured in $CDCl_3$.

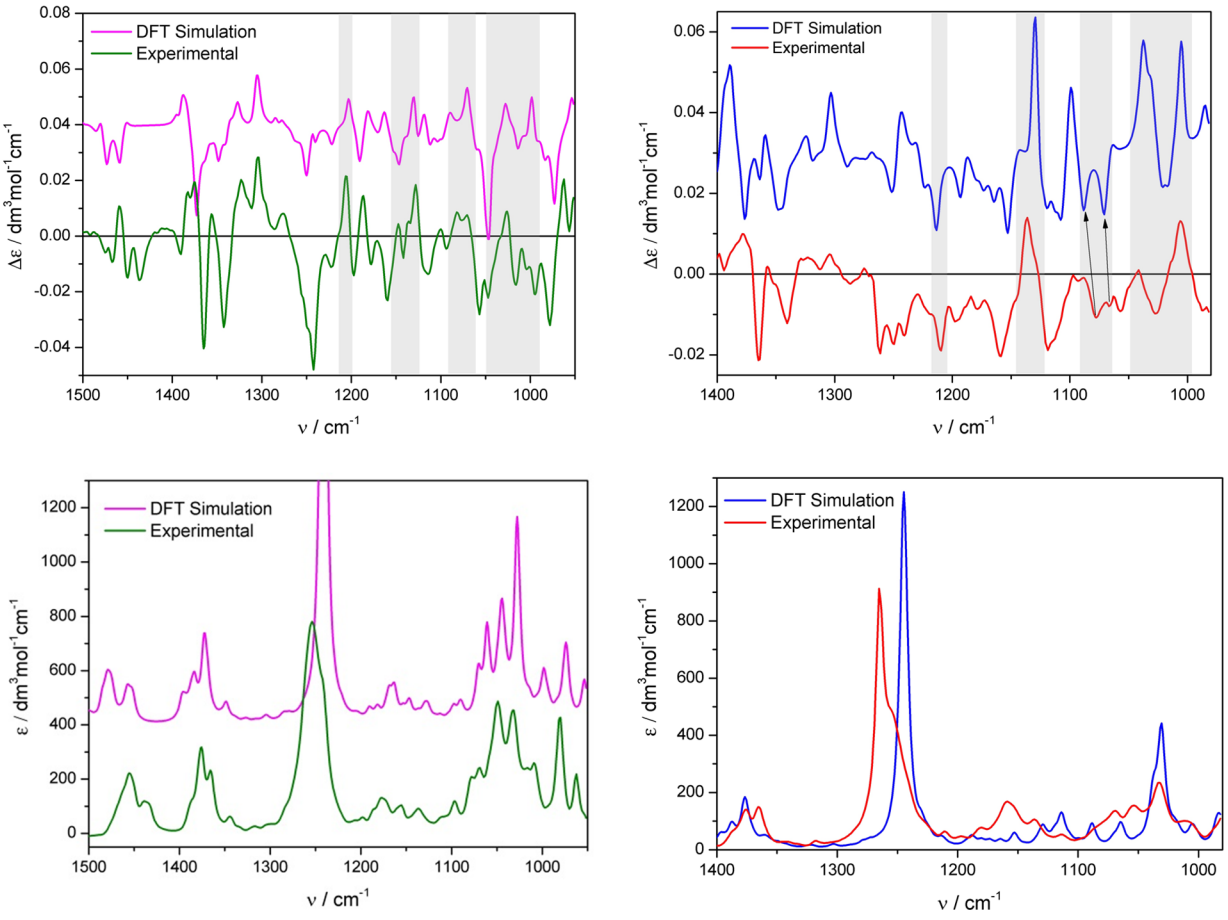

Figure 17. Comparison of experimental and simulated VCD and IR spectra of diosgenin acetate (left) and 22-isodiosgenin acetate (**17**) (right).

An additional proof of this assignment comes from vibrational circular dichroism (VCD) spectroscopy. As can be seen in Figure 16, the VCD spectra of diosgenin acetate and its 22-iso derivative **17** substantially differ in the fingerprint region facilitating the sterochemical assignment. Differences occurring in the range of C−O stretching vibration in the E and F rings as well as C−H wagging and twisting vibrations are highlighted in the Figure 16. The calculated VCD and IR spectra are compared in Figure 17.

As one can see, the overall agreement of the predicted and experimental spectra supports the stereochemical assignment of 22-isodiosgenin acetate (**17**). Therefore, one can say that such a combined use of different chiroptical methods for structure determination allows for an unambiguous configurational assignment.

■ CONCLUSIONS

The first synthesis of sapogenin derivatives with inverted configuration at the spiro carbon atom from 25*R*- and 25*S*-23-oxosapogenins is described. The isomerization reactions were carried out by irradiation of the starting ketones with a UV lamp. The obtained 22-iso compounds were proved relatively stable in the solid state but in solution underwent isomerization to ketones with a natural configuration at C22, particularly under acidic conditions. In the case of a 22-isosapogenin devoid

dx.doi.org/10.1021/jo3022549 | J. Org. Chem. 2012, 77, 11257−11269

of the 23-oxo group (22-isodiosgenin acetate) isomerization to the natural sapogenin was even faster. This observation may explain why compounds extracted from natural sources show always the configuration at C22 characteristic for the more stable isomers.

The results of combined experimental and theoretical analysis of ECD spectra of sapogenins **9**–**14**, consistent with NMR predictions, allowed the assignment of their three-dimensional molecular structure with great certainty. Moreover, theoretical VCD spectra of diosgenin acetate and its derivative **17** show the same tendency as the experimental data, further confirming the configurational assignment derived from the ECD spectra. Thus, the methodology consisting of concerted DFT calculations of ECD and VCD spectra to solve structural and stereochemical problems has demonstrated again its potential and excellent effectiveness.

EXPERIMENTAL SECTION

General Information. Melting points were determined on a Kofler apparatus of the Boetius type. NMR spectra were recorded on a 400 MHz spectrometer in $CDCl_3$ as a solvent with TMS as internal standard (only selected signals in the ^{1}H NMR spectra are reported). Infrared spectra were recorded on a FT-IR spectrometer in chloroform solutions. Mass spectra were recorded on a time-of-flight (TOF) spectrometer with electrospray ionization (ESI). The reaction products were isolated by column chromatography performed on 70–230 mesh silica gel. The progress of reactions was monitored using silica gel 60 TLC plates. TLC spots were visualized by heating plates that were sprayed with ammonium molybdate/cerium(IV) sulfate solution.

23-Oxotigogenin acetate (**9**), 23-oxodiosgenin acetate (**10**), and 23-oxosarsasapogenin acetate (**11**) were prepared by an improved Barton's procedure.[14,15]

Photochemical studies were carried out using the Heraeus photochemical reactor, which consisted of a submerged UV lamp (TQ 150 type; high pressure mercury burner, 150 W power input) surrounded by a quartz shield. A stirred solution of 23-oxosapogenin (**9**, **10**, or **11**; ∼100 mg) in 400 mL of the acetonitrile/dichloromethane mixture (9:1) in the presence of triethylamine (1.5 mL) was irradiated at room temperature for approximately 2 h. The reactions were monitored by TLC every 15 min. The solvents were evaporated in vacuo after the reaction, and products were separated by a silica gel column chromatography.

*23-Oxo-22-isotigogenin Acetate (**12**) from 23-Oxotigogenin Acetate (**9**).* Irradiation time: 2 h. Elution with 6% EtOAc/hexane afforded the unreacted compound **9** (40 mg; 40%) followed by compound **12** (30 mg; 30%); colorless crystals: mp 254–257 °C; IR (ν, cm^{-1}) 1721, 1262, 1027; ^{1}H NMR (ppm) 4.64 (m, 1H), 4.20 (m, 1H), 4.13 (dd, J = 11.2, 3.5 Hz, 1H), 3.54 (ddd, J = 11.2, 3.8, 1.7 Hz, 1H), 2.73 (dd, J = 15.8, 5.5 Hz, 1H), 1.97 (s, 3H), 1.06 (d, J = 6.9 Hz, 3H), 1.03 (d, J = 7.1 Hz, 3H), 0.84 (s, 3H), 0.83 (s, 3H); ^{13}C NMR (ppm) 203.8 (C), 170.7 (C), 111.1 (C), 82.1 (CH), 73.6 (CH), 68.1 (CH_2), 61.0 (CH), 55.6 (CH), 54.1 (CH), 44.6 (CH), 43.7 (CH_2), 40.9 (CH), 40.8 (C), 40.0 (CH_2), 36.7 (CH_2), 35.6 (C), 35.0 (CH), 34.0 (CH_2), 32.1 (CH_2 x 2), 30.2 (CH), 28.4 (CH_2), 27.4 (CH_2), 21.4 (CH_3), 21.0 (CH_2), 17.9 (CH_3), 16.6 (CH_3), 14.9 (CH_3), 12.2 (CH_3); MS-ESI (m/z) 495.7 (MNa^+). Anal. Calcd for $C_{29}H_{44}O_5$: C, 73.69; H, 9.38. Found: C, 73.48; H, 9.45.

*23-Oxo-22-isodiosgenin Acetate (**13**) from 23-Oxodiosgenin Acetate (**10**).* Irradiation time: 1.5 h. Elution with 6% EtOAc/hexane afforded the unreacted compound **10** (60 mg; 60%) followed by compound **13** (20 mg; 20%); colorless crystals: mp 214–217 °C; IR (ν, cm^{-1}) 1723, 1255, 1032; ^{1}H NMR (ppm) 5.37 (m, 1H), 4.60 (m, 1H), 4.27 (m, 1H), 4.20 (dd, J = 11.2, 3.4 Hz, 1H), 3.60 (ddd, J = 11.2, 3.8, 1.8 Hz, 1H), 2.78 (dd, J = 15.9, 5.4 Hz, 1H), 2.03 (s, 3H), 1.10 (d, J = 7.0 Hz, 3H), 1.07 (d, J = 7.1 Hz, 3H), 1.04 (s, 3H), 0.88 (s, 3H); ^{13}C NMR (ppm) 203.8 (C), 170.5 (C), 139.7 (C), 122.2 (CH), 111.2 (C), 82.1 (CH), 73.8 (CH), 68.1 (CH_2), 60.9 (CH), 55.8 (CH), 49.9 (CH), 43.7 (CH_2), 40.9 (CH), 40.5 (C), 39.7 (CH_2), 38.1 (CH_2), 36.9 (CH_2), 36.7 (C), 32.2 (CH_2), 32.0 (CH_2), 31.3 (CH), 30.2 (CH), 27.7 (CH_2), 21.4 (CH_3), 20.8 (CH_2), 19.3 (CH_3), 17.9 (CH_3), 16.4 (CH_3), 14.9 (CH_3); MS-ESI (m/z) 493.6 (MNa^+). Anal. Calcd for $C_{29}H_{42}O_5$: C, 74.01; H, 8.99. Found: C, 73.82; H, 9.09.

*23-Oxo-22-isosarsasapogenin Acetate (**14**) from 23-Oxosarsasapogenin Acetate (**11**).* Irradiation time: 2 h. Elution with 1.5% EtOAc/benzene afforded the unreacted compound **11** (44 mg; 44%) followed by compound **14** (20 mg; 20%); colorless crystals: mp 152–154 °C; IR (ν, cm^{-1}) 1724, 1452, 1263; ^{1}H NMR (ppm) 5.07 (m, 1H), 4.16 (m, 1H), 3.78 (ddd, J = 11.3, 4.6, 1.9 Hz, 1H), 3.72 (t, J = 11.3 Hz, 1H), 2.05 (s, 3H), 1.06 (d, J = 7.1 Hz, 3H), 0.99 (s, 3H), 0.92 (d, J = 6.4 Hz, 3H), 0.84 (s, 3H); ^{13}C NMR (ppm) 202.5 (C), 170.6 (C), 110.1 (C), 81.7 (CH), 70.7 (CH), 68.9 (CH_2), 60.8 (CH), 55.8 (CH), 44.4 CH_2), 40.9 (C), 40.8 (CH), 40.2 (CH_2), 40.0 (CH), 37.3 (CH), 35.2 (CH), 35.0 (C), 32.1 (CH_2), 31.9 (CH), 30.7 (CH_2), 30.6 (CH_2), 26.4 (CH_2 x 2), 25.0 (CH_2), 23.8 (CH_3), 21.5 (CH_3), 20.9 (CH_2), 16.7 (CH_3), 16.6 (CH_3), 14.4 (CH_3); MS-ESI (m/z) 495.3 (MNa^+). Anal. Calcd for $C_{29}H_{44}O_5$: C, 73.69; H, 9.38. Found: C, 73.47; H, 9.51.

*Deoxygenation of Compound **13**.* 23-Oxo-22-isodiosgenin acetate (**13**; 125 mg) was subjected to reduction with $NaBH_4$ (65 mg) in methanol (15 mL) for 16 h at room temperature. The standard workup of the reaction mixture afforded epimeric alcohols **15** (115 mg, 0.24 mmol), which were dissolved in dry THF (10 mL) and treated with sodium hydride (20 mg) and imidazole (5 mg) under Ar. The mixture was stirred at room temperature for 2 h. Carbon disulfide (0.043 mL, 3 equiv) and methyl iodide (0.045 mL, 3 equiv) were added sequentially (20 min) under Ar. The reaction mixture was stirred for 0.5 h, poured into aqueous NH_4Cl and extracted with Et_2O. The organic layer was dried over Na_2SO_4. Silica gel column chromatography afforded xanthate **16** (17 mg, 12% yield) as a yellowish oil eluted with 8% AcOEt in hexane: IR (ν, cm^{-1}) 1725, 1254, 1232; ^{1}H NMR (ppm) 5.80 (dd, J = 10.6, 5.4 Hz, 1H), 5.39 (m, 1H), 4.78 (m, 1H), 4.62 (m, 2H), 4.08 (dd, J = 11.2, 2.9 Hz, 1H), 3.38 (d, J = 11.2 Hz, 1H), 2.58 (s, 3H), 2.04 (s, 3H), 1.19 (d, J = 7.0 Hz, 3H), 1.06 (s, 3H); 1.02 (d, J = 7.4 Hz, 3H), 0.92 (s, 3H); ^{13}C NMR (ppm) 214.7 (C), 170.5 (C), 139.8 (C), 122.3 (CH), 111.3 (C), 83.9 (CH), 79.0 (CH), 73.9 (CH), 67.5 (CH_2), 62.6 (CH), 55.7 (CH), 50.0 (CH), 42.6 (CH), 40.9 (C), 39.8 (CH_2), 38.1 (CH_2), 37.0 (C), 36.7 (CH_2), 33.6 (CH_2), 32.0 (CH_2), 31.3 (CH), 29.8 (CH_2), 29.5 (CH), 27.7 (CH_2), 21.4 (CH_3), 20.8 (CH_2), 19.3 (CH_3), 19.2 (CH_3), 16.7 (CH_3), 16.4 (CH_3), 16.1 (CH_3); HRMS (ESI-TOF) m/z [M + Na]$^+$ calcd for $C_{31}H_{46}O_5S_2Na$ 585.2684, found 585.2671.

To xanthate **16** (17 mg, 0.03 mmol) in dry toluene (10 mL) tri-*n*-butyltin hydride (0.17 mL, 2.5 equiv) was added under Ar. The reaction mixture was refluxed for 1 h. The organic solvent was evaporated in vacuo; the reaction mixture was poured into water and extracted with dichloromethane. The organic layer was dried over Na_2SO_4. The silica gel column chromatography afforded isodiosgenin acetate **17** (6 mg, 43% yield) eluted with 3% AcOEt in hexane, colorless crystals: mp 159–162 °C; IR (ν, cm^{-1}) 1724, 1255, 1255; ^{1}H NMR (ppm) 5.38 (m, 1H), 4.61 (m, 2H), 4.32 (m, 1H), 4.06 (dd, J = 11.2, 3.2 Hz, 1H), 3.38 (d, J = 11.2 Hz, 1H), 2.04 (s, 3H), 1.06 (d, J = 7.3 Hz, 3H), 1.05 (s, 3H), 1.01 (d, J = 7.2 Hz, 3H), 0.92 (s, 3H); ^{13}C NMR (ppm) 170.5 (C), 139.7 (C), 122.3 (CH), 111.2 (C), 80.8 (CH), 73.9 (CH), 68.6 (CH_2), 62.3 (CH), 55.5 (CH), 50.1 (CH), 41.5 (CH), 40.8 (C), 40.3 (CH_2), 38.1 (CH_2), 37.0 (CH_2), 36.8 (C), 32.9 (CH_2), 32.1 (CH_2), 31.1 (CH), 27.7 (CH_2), 27.5 (CH), 25.5 (CH_2), 23.4 (CH_2), 21.4 (CH_3), 20.9 (CH_2), 19.3 (CH_3), 16.9 (CH_3), 16.4 (CH_3 x 2); HRMS (ESI-TOF) m/z [M + Na]$^+$ calcd for $C_{29}H_{44}O_4Na$ 479.3137, found 479.3127.

Crystal Structure Determination. Suitable crystals for X-ray analysis of **12** were obtained from dichloromethane by slow evaporation of the solvent; monoclinic, space group $P2_1$ with two molecules in the unit cell.

The X-ray data collection was performed at 273 K on a Kappa CCD diffractometer ($\lambda_{MoK\alpha}$ = 0.71073 Å, monochromator: graphite). Refinement and data output were carried out with SHELXL-97 program included in the software package WingGX-Version 1.80.05.

dx.doi.org/10.1021/jo3022549 | J. Org. Chem. 2012, 77, 11257–11269

Crystallographic data have been deposited at the Cambridge Crystallographic Center as Supporting Information No. 906258. A copy of the data can be obtained free of charge by correspondence to CCDC, 12 Union Road, Cambridge CB2 1EZ, UK. E-mail: deposit@ccdc.cam.ac.uk.

The molecular structure of **12** with displacement ellipsoids drawn at the 35% probability level is shown in Figure 6.

The packing structure of **12** (see the Supporting Information) is characterized by an arrangement of one-dimensional layers propagating along the plane formed by the *a* and *c* crystallographic axis that is governed by the weak intermolecular hydrogen bond between 25-H and the oxygen O28 atom of a neighboring molecule, with a C25−(25-H)···O28 angle of 143° and a C25−O28 distance of 3.433(5) Å with symmetry code [1566.] = *x*, 1 + *y*, 1 + *z*. Also the supramolecular arrangement shows two moderate intramolecular hydrogen bond interactions between 3-H and O28 with a C3−(3-H)···O28 angle of 102° and a C3−O28 distance of 2.680(4) Å and the interaction of 21A-H and O23 with a C21−(21A-H)···O23 angle of 116° and a C21−O23 distance of 2.971(4) Å (Figure 8). All of these interactions are nonclassical hydrogen bonds, since the donor is a carbon atom (Steiner[24] and Desiraju[25]).

ECD Measurements. The electronic circular dichroism (ECD) spectra were recorded between 450−180 nm at room temperature in spectroscopic grade acetonitrile. Solutions of **9**−**14** with concentrations in the range from 3.6×10^{-4} to 4.5×10^{-4} M were examined in quartz cell with path length of 2−0.1 cm. In the case of diosgenin acetate and 22-isodiosgenin acetate (**17**) concentrations were higher (from 7.4×10^{-4} to 8.0×10^{-4} M). All spectra were recorded using 100 nm/min scanning speed, a step size of 0.2 nm, a bandwidth of 1 nm, a response time of 0.5 s, and an accumulation of 5 scans. The spectra were background corrected.

Low-temperature ECD measurement of **12** were performed in the temperature range 293−93 K in solution of MI_{13} (methylcyclohexane/isopentane, 1:3, by vol.) as a solvent. Solution with concentrations 8.8×10^{-4} M was measured between 400−220 nm in 1 cm quartz cell. Baseline correction was achieved by subtracting the spectrum of a reference MI_{13} obtained under the same conditions. All spectra were normalized to $\Delta\varepsilon$ using volume correction for MI_{13}.

The ECD solid-state spectrum of **12** was obtained using diffused transmission (DTCD) mode, as KCl pellet placed in the integrating sphere coated with barium sulfate and introduced to the high sensitivity photomultiplier tube situated at 90°. ECD spectrum (1.318 mg/100 mg KCl) was recorded between 450−250 nm at room temperature using the following parameters: 100 nm/min scanning speed, a step size of 0.2 nm, a bandwidth of 5 nm, a response time of 0.5 s, and an accumulation of 5 scans. The resulting spectrum was background corrected. The KCl pellet was mounted on a rotatable holder located just before the integrating sphere. The sample was measured upon rotation of the disk around the incident axis direction at various rotation angles. The spectra were almost identical, demonstrating the absence of detectable spectral artifacts. Linear dichroism (LD) was also measured; the order was ca. 2×10^{-3}.

VCD Measurements. The IR and VCD spectra of diosgenin acetate and **17** were measured at a resolution of 4 cm^{-1} using $CDCl_3$. FT-VCD spectrometer was equipped with dual sources and dual PEM's. Concentrations were 0.13 and 0.04 M, respectively, the cell path length was 102 μm, and the probes were placed in a BaF_2 cell with a path length of 102 μm and assembled in rotating holder (14 s/cycle). The ZnSe photo elastic modulator of the instrument was set to 1400 cm^{-1}. To improve the S/N ratio, the spectra were measured for 4 h 40 min (14336 scans) and 21 h (65536 scans), respectively. Baseline correction was achieved by subtracting the spectrum of a reference $CDCl_3$ obtained under the same conditions.

Quantum Chemical Calculations. *Conformational Analysis and TD DFT Optimization.* The conformational search was done using HyperChem program[26] with MM+ force field within 3 kcal/mol energy windows, and then all structures were submitted to the Gaussian09 program[27] for a single-point energy calculation at B3LYP/6-31G(d) TD DFT level of theory in order to improve confidence for conformers found. Then, finally the prediction of ECD and UV spectra were performed.

UV/ECD Calculations. Simulation of UV/ECD spectra were carried out with TD DFT method for conformer/conformers found in two-step conformation analysis. The B3LYP hybrid functional in conjunction with the Ahlrichs' triple-ζ split-valence basis set TZVP was used. For reflecting the solvent influence on measured ECD spectra, the polarizable continuum model (PCM) implemented in the Gaussian 09 was used. Rotatory strengths were calculated using both length and velocity representations. The differences between the length and velocity of calculated values of rotatory strengths were <3%, and for this reason, only the velocity representations (R_{vel}) were taken into account. The ECD spectra were simulated by overlapping Gaussian functions for each transition by means of the SpecDis[28] program. The final spectra were Boltzmann averaged (T = 298 K) according to the population percentages of individual conformers based on the relative Gibbs free energies (ΔG). The same results were obtained using ΔE^{SCF} and ΔH values from Gaussian output file. The calculated UV spectra were red-shifted by 10−15 nm in relation to the experimental, and consequently ECD spectra were also wavelength corrected. A Gaussian band-shape was applied with 0.35−0.38 eV as a half-height width.

IR/VCD Calculations. Computations were performed in the framework of TD-DFT in Gaussian 09 package.[27] In order to predict VCD spectra for diosgenin acetate and 22-isodiosgenin acetate (**17**), first geometry was reoptimized, and then calculations of harmonic vibrational frequencies, dipole strengths and rotational strengths were carried out at the same level. B3LYP hybrid functional was tested in conjunction with the 6-31G(d), TZVP and DGDZVP basis sets. Calculated IR and VCD spectra were extracted from Gaussian 09 output to ASCII XY-format by using ViewVCD software[29] (Lorentzian curves were simulated using half-width at half-height values of 6 cm^{-1}). Comparisons between theoretical and measured IR and VCD spectra were evaluated using CompareVOA confidence level algorithm.[30] The best comparison was obtained in the case of combination B3LYP/DGDZVP. Therefore, only these data are presented here.

Summary for diosgenin acetate: scaled factor = 0.975; IR spectral similarity = 82.2%; VCD similarity for the correct enantiomer (22*R*) = 80.0%; enantiomer similarity index (calculated as a difference between similarity for the correct enantiomer and opposite one) = 56.1%; confidence level for the stereochemical assignment (22*R*) = 100%.

Summary for **17**: scaled factor = 0.977; IR spectral similarity = 72.0%; VCD similarity for the correct enantiomer (22*S*) = 77.2%, enantiomer similarity index = 52.2%, confidence level for the stereochemical assignment (22*S*) = 100%

■ ASSOCIATED CONTENT

Ⓢ Supporting Information

Spectroscopic data for compounds **12**−**17**, CD analysis, DFT calculations, and crystallographic information file (CIF) for compound **12**. This material is available free of charge via the Internet at http://pubs.acs.org.

■ AUTHOR INFORMATION

Corresponding Author

*Tel.: +48 85 7457585. Fax: +48 85 7457581. E-mail: morzycki@uwb.edu.pl.

Notes

The authors declare no competing financial interest.

■ ACKNOWLEDGMENTS

Financial support from the Polish Ministry of Science and Higher Education (Grant No. BST-124) is gratefully acknowledged. One of the authors (M.G.) acknowledges the financial support of the National Science Centre, Poland, Grant No. 2011/03/N/ST4/02426 and also Grant No. G34-15 for computational time at the Interdisciplinary Centre for

Mathematical and Computational Modelling (ICM) of University of Warsaw, Poland. The Heraeus reactor equipped with TQ 150 type UV lamp was funded by EU, as part of the Operational Program Development of Eastern Poland 2007-2013, Project POPW.01.03.00-20-034/09-00.

REFERENCES

(1) Hostettmann, K.; Marston, A. *Saponins*; University Press: Cambridge, UK, 1995.
(2) (a) Fieser, L.; Fieser, M. Sapogenins. In *Steroids*; Reinhold Publishing Corporation: New York, 1959; Chapter 21. (b) Marker, R. E.; Rohrmann, E. *J. Am. Chem. Soc.* **1940**, *62* (518−520), 898−900.
(3) Marker, R. E.; Rohrmann, E. *J. Am. Chem. Soc.* **1939**, *61*, 3592−93.
(4) (a) Torgov, I. V. *Chemistry of Spirostanols (in Russian)*; Nauka: Moscow, 1986. (b) Fried, J.; Edwards, J. A. *Organic Reactions in Steroid Chemistry*; van Nostrand Reinhold Company: New York, 1972; Vol. *2*, Chapter 11. (c) Jastrzębska, I. *Curr. Org. Chem.* **2012**, *16*, 353−372.
(5) (a) Lee, S.; LaCour, T. G.; Fuchs, P. L. *Chem. Rev.* **2009**, *109*, 2275−2314. (b) Phillips, S. T.; Shair, M. D. *J. Am. Chem. Soc.* **2007**, *129*, 6589−6598. (c) Pettit, G. R.; Inoue, M.; Kamano, Y.; Herald, D. L.; Arm, C.; Dufresne, C.; Christie, N. D.; Schmidt, J. M.; Doubek, D. L.; Krupa, T. S. *J. Am. Chem. Soc.* **1988**, *110*, 2006−2007. (d) Fukuzawa, S.; Matsunaga, S.; Fusetani, N. *J. Org. Chem.* **1994**, *59*, 6164−6166. (e) Iglesias-Arteaga, M. A.; Morzycki, J. W. Cephalostatins and Ritterazines. In *The Alkaloids: Chemistry and Biology*; Knölker, H.-J., Ed.; Elsevier: Amsterdam; Vol. *72*, Chapter 2, in press.
(6) Iglesias-Arteaga, M. A.; Jastrzębska, I.; Morzycki, J. W. *Pol. J. Chem.* **2006**, *80*, 667−671.
(7) Tabori, A.; Teshima, M.; Koyanagi, J.; Kawase, M.; Miyamae, H.; Yoza, K.; Takasaki, A.; Nagamura, Y.; Saito, S. *Eur. J. Med. Chem.* **2000**, *35*, 511−527.
(8) Morzycki, J. W.; López, Y.; Płoszyńska, J.; Santillan, R.; Siergiejczyk, L.; Sobkowiak, A. *J. Electroanal. Chem.* **2007**, *610*, 205−210.
(9) (a) Scheer, I.; Kostic, R. B.; Mosettig, E. *J. Am. Chem. Soc.* **1953**, *75*, 4871−4872. (b) Callow, R. K.; Massy-Beresford, P. N. *J. Chem. Soc.* **1958**, 2645−2653.
(10) (a) Woodward, R. B.; Sondheimer, F.; Mazur, Y. *J. Am. Chem. Soc.* **1958**, *80*, 6693−6694. (b) Seo, S.; Uomori, A.; Takeda, K. *J. Org. Chem.* **1986**, *51*, 3823−3827.
(11) Pettit, G. R.; Xu, J. P.; Schmidt, J. M.; Boyd, M. R. *Bioorg. Med. Chem. Lett.* **1995**, *5*, 2027−2032.
(12) LaCour, T. G. Steroidal Anticancer Agents. Ph.D. Thesis, Purdue University, 2001.
(13) Flessner, T.; Jautelat, R.; Scholz, U.; Winterfeldt, E. *Fortschr. Chem. Org. Naturst.* **2004**, 1−80.
(14) Barton, D. H. R.; Taylor, P. G.; Werstiuk, E. *J. Chem. Soc. C* **1970**, 1977−1981.
(15) Arteaga-Iglesias, M. A.; Gil, R. P.; Martinez, C. S. P.; Manchado, F. C. *Synth. Commun.* **2000**, *30*, 163−170.
(16) Agrawal, P. K.; Bunsawansong, P.; Morris, G. A. *Phytochemistry* **1998**, *47*, 255−257.
(17) (a) Kołodziejska, R.; Górecki, M.; Frelek, J.; Dramiński, M. *Tetrahedron: Asymmetry* **2012**, *23*, 683−689. (b) Polavarapu, P. L.; Frelek, J.; Woźnica, M. *Tetrahedron: Asymmetry* **2011**, *22*, 1720−1724. (c) Krohn, K.; Kouam, S. F.; Kuigoua, G. M.; Hussain, H.; Cludius-Brandt, S.; Flörke, U.; Kurtán, T.; Pescitelli, G.; Di Bari, L.; Draeger, S.; Schulz, B. *Chem.—Eur. J.* **2009**, *15*, 12121−12132. (d) Di Bari, L.; Pescitelli, G.; Salvadori, P.; Rovini, M.; Anzini, M.; Cappelli, A.; Vomero, S. *Tetrahedron: Asymmetry* **2006**, *17*, 3430−3436.
(18) (a) Laue, T.; Plagens, A. *Named Organic Reactions*, 2nd ed.; John Wiley & Sons, Ltd: New York, 2005; pp 212−215. (b) Bohne, C. Norrish Type I Processes of Ketones: Basic Concepts. In *CRC Handbook of Photochemistry and Phytobiology*; Horspool, W. M.; Song, P.-S., Eds.; CRC Press Inc.: Boca Raton, FL, 1995; pp 416−422.
(19) Jastrzębska, I.; Morzycki, J. W.; Trochimowicz, U. *Tetrahedron Lett.* **2004**, *45*, 1929−1932.
(20) For comparison to the hydride reduction of the 23-carbonyl group in the normal spirostane systems, see: Anulewicz-Ostrowska, R.; Jastrzębska, I.; Morzycki, J. W.; Wójcik, J. *J. Org. Chem.* **2002**, *67*, 6916−6924.
(21) Betancor, C.; Dorta, R. L.; Freire, R.; Martín, A.; Prangé, T.; Suárez, E. *J. Org. Chem.* **1998**, *63*, 6355−6362.
(22) Barton, D. H. R.; McCombie, S. *J. Chem. Soc., Perkin 1* **1975**, 1574−1585.
(23) Barton, D. H. R.; Stick, R. V.; Subramanian, R. *J. Chem. Soc., Perkin 1* **1976**, 2112−2116.
(24) Steiner, T. *Angew. Chem., Int. Ed.* **2002**, *41*, 48−76.
(25) (a) Desiraju, G. R. *Acc. Chem. Res.* **1996**, *29*, 441−449. (b) Steiner, T. *Chem. Commun.* **1997**, 727−734.
(26) *HyperChem 8.0 Professional ed.*; Hypercube, Inc.: Gainesville, FL.
(27) Frisch, M. J.; Trucks, G. W.; Schlegel, H. B.; Scuseria, G. E.; Robb, M. A.; Cheeseman, J. R.; Scalmani, G.; Barone, V.; Mennucci, B.; Petersson, G. A.; Nakatsuji, H.; Caricato, M.; Li, X.; Hratchian, H. P.; Izmaylov, A. F.; Bloino, J.; Zheng, G.; Sonnenberg, J. L.; Hada, M.; Ehara, M.; Toyota, K.; Fukuda, R.; Hasegawa, J.; Ishida, M.; Nakajima, T.; Honda, Y.; Kitao, O.; Nakai, H.; Vreven, T.; Montgomery, J. A. Jr.; Peralta, J. E.; Ogliaro, F.; Bearpark, M.; Heyd, J. J.; Brothers, E.; Kudin, K. N.; Staroverov, V. N.; Kobayashi, R.; Normand, J.; Raghavachari, K.; Rendell, A.; Burant, J. C.; Iyengar, S. S.; Tomasi, J.; Cossi, M.; Rega, N.; Millam, J. M.; Klene, M.; Knox, J. E.; Cross, J. B.; Bakken, V.; Adamo, C.; Jaramillo, J.; Gomperts, R.; Stratmann, R. E.; Yazyev, O.; Austin, A. J.; Cammi, R.; Pomelli, C.; Ochterski, J. W.; Martin, R. L.; Morokuma, K.; Zakrzewski, V. G.; Voth, G. A.; Salvador, P.; Dannenberg, J. J.; Dapprich, S.; Daniels, A. D.; Farkas, Ö.; Foresman, J. B.; Ortiz, J. V.; Cioslowski, J.; Fox, D. J. *Gaussian 09*, Revision A.02; Gaussian, Inc.: Wallingford, CT, 2009.
(28) Bruhn, T.; Hemberger, Y.; Schaumlöffel, A.; Bringmann, G. *Specdis* v. 1.53; University of Würzburg: Würzburg, Germany, 2012.
(29) *ViewVCD software*; BioTools, Inc.: Jupiter, FL, 2010.
(30) Debie, E.; Bultinck, P.; Nafie, L. A. *CompareVOA software*, BioTools, Inc.: Jupiter, FL, 2010.